Mechanisms responsible for the initiation of a fast breakdown in an atmospheric discharge

To cite this article before publication: Egor Parkevich *et al* 2018 *Plasma Sources Sci. Technol.* in press https://doi.org/10.1088/1361-6595/aaebdb

Mechanisms responsible for the initiation of a fast breakdown in an atmospheric discharge

E V Parkevich[1,2], G V Ivanenkov[1], M A Medvedev[1,2], A I Khirianova[1,2], A S Selyukov[1], A V Agafonov[1], A R Mingaleev[1], T A Shelkovenko[1] and S A Pikuz[1]

[1] Lebedev Physical Institute of the Russian Academy of Sciences, Leninsky Avenue 53, Moscow 119991, Russia
[2] Moscow Institute of Physics and Technology, Institutskiy Pereulok 9, Dolgoprudny, Moscow Region 141700, Russia

E-mail: parkevich@phystech.edu
August 2018

Abstract. The initial stage of the fast electrical breakdown of an air gap with a pin-to-plane electrode geometry is studied on a nanosecond time scale using multi-frame laser probing with an exposure time of 70 ps and spatial resolution as high as 3–4 μm. We find that the gap breakdown is associated with the fast ($\lesssim$ 1 ns) formation of a micron-sized ($\sim$ 10 μm) cathode spot that appears as a plasma with an electron density of $n_e \approx 10^{19}$ cm^{-3}. The spot is then transformed into a spark channel having an electron density of $n_e \sim 10^{19}$–10^{20} cm^{-3}. Within $\sim$ 1 ns after the breakdown the dynamics of the highly ionized near-cathode plasma governs the current capacity of the discharge gap as well as the current rise rate.

Submitted to: *Plasma Sources Sci. Technol.*

In spite of the fact that the atmospheric discharge has been studied for more than a century [1, 2], each newly developed diagnostic technique or a combination of the conventional ones provides a new insight into the physics behind the plasma formation processes. In particular, this is the case for the spark discharge, which is most frequently encountered in practice or in laboratory experiments. Generally, sparks [3] are understood as highly ionized and conductive current channels that appear in a discharge and are accompanied by a significant increase in the discharge current. It was proposed in Ref. [4] that the spark channel originating from the cathode surface is associated with the explosive processes accompanied by the appearance of an erosion plasma. In addition to that, the initiation of the gap breakdown can depend on the emission properties of the cathode surface [5, 6]. However, still it is impossible to develop a comprehensive model of the spark formation as the investigation of the corresponding stage of the discharge evolution is a complicated technical problem. Here the main difficulties arise due to the small size ($\sim$ 1–10 μm) of the regions of the spark formation as well as due to subnanosecond time scales of the near-cathode plasma evolution [4, 6, 7, 8]. Thus, it is challenging to obtain the quantitative information on the near-cathode plasma with high spatial and temporal resolution.

In order to accomplish this task, in this Letter we trace the process of the spark channel formation by using multi-frame laser probing with an exposure time of 70 ps and spatial resolution as high as 3–4 μm. We find that the electrical breakdown of an air gap is associated with the fast ($\lesssim$ 1 ns) formation of a highly ionized near-cathode plasma with an electron density of $n_e \approx 10^{19}$ cm^{-3} in micron-sized ($\sim$ 10 μm) regions at the cathode surface. This plasma is then transformed into a spark channel having an electron density of $n_e \sim 10^{19}$–10^{20} cm^{-3}. The findigs indicate that within $\sim$ 1 ns after the breakdown the dynamics of the highly ionized near-cathode plasma governs the current capacity of the discharge gap as well as the current rise rate.

The experiments were carried out on an installation involving a high-voltage generator triggered by an ignition laser beam with jitter as low as 1 ns and a laser probing system. The generator provided a 25 kV output pulse with a duration up to 40 ns and a rise time of $\approx$ 4 ns. The maximum discharge current was $I_0 \approx 330$ A. A Lotis LS-2151 Nd: YAG laser with 1064 and 532 nm emission and the pulse energy up to 80 mJ was employed. A part of the laser beam energy ($\approx$ 90%, both harmonics) was used to trigger the high-voltage generator. The rest of the radiation ($\approx$ 10%, second harmonic only) was used for probing the discharge. The laser pulse duration was 70 ps at 532 nm.

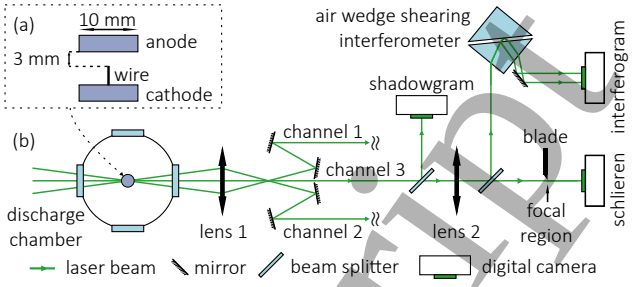

Figure 1. Discharge gap (a). Laser probing system (b).

A three-frame optical system (Fig. 1) having 4x magnification was developed for simultaneous recording of interference, shadow and schlieren images [9] of the discharge gap. An air wedge shearing interferometer [10] was employed to record the interferograms. "Era-14" and "Era-7" lenses (lenses 1 and 2 in Fig. 1) [11] with resolutions of 500 and 450 lp/mm, focal lengths of 135 and 105 mm and equal f-numbers of F2.8 were used to collect the probing beams. These lenses also have low astigmatism at oblique incidence. Therefore, three probing beams were collected using a single lens (lens 1 in Fig. 1) and, thus, the optical system was greatly simplified. Two of the three beams were directed at small angles ($\approx 3^\circ$) to the main optical axis. The average interval between the probing beams was $\approx$2 ns. The spatial resolution of the "channel 3" was $\approx$ 3 μm ($\approx$ 70% of the diffraction limit), and the other two channels had the resolution of $\approx$ 4 μm. The images were recorded by digital cameras (Canon EOS 1100D). A photodetector (Thorlabs DET10A/M) with a rise time of 1 ns was used to time the arrival of the probing beams. The discharge current and the gap voltage were measured using an anode shunt and a capacitive voltage divider. The signals from the detectors were recorded by 500 MHz digital oscilloscopes (Tektronix TDS3054B).

The atmospheric discharge was studied using the "pin-to-plane" electrode geometry (Fig. 1). The point cathode was fabricated using thin copper wires. The gap between the wire (2 mm in length) and plane copper anode was 3 mm. The employed gap geometry provided a strong field near the cathode and a spark originating from the wire end. Consequently, introduction of the point cathode dramatically improved the adjustment accuracy of the optical system, which was focused on the spark.

It was found that approximately 0.5 ns after the breakdown a cathode spot (Fig. 2) appears at the top of the point cathode. Here the breakdown corresponds to a sharp increase ($dI/dt \sim 100$ A/ns) in the discharge current. The spot has a size of $\sim$ 10 μm and appears as

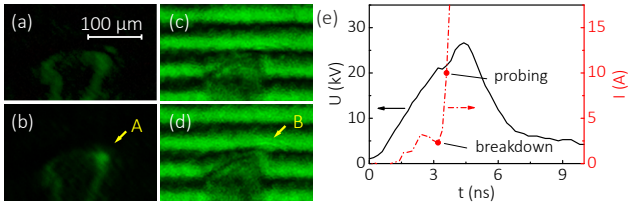

Figure 2. Shot no. 1. Shlieren-images (a,b) and interferograms (c,d) obtained before discharge (a,c) and 0.5 ns (b,d) after breakdown; A—cathode spot, B—plasma with electron density of $n_e \approx 10^{19}$ cm^{-3}. Diameter of copper cathode was 50 μm. Discharge characteristics (e): U—gap voltage, I—discharge current.

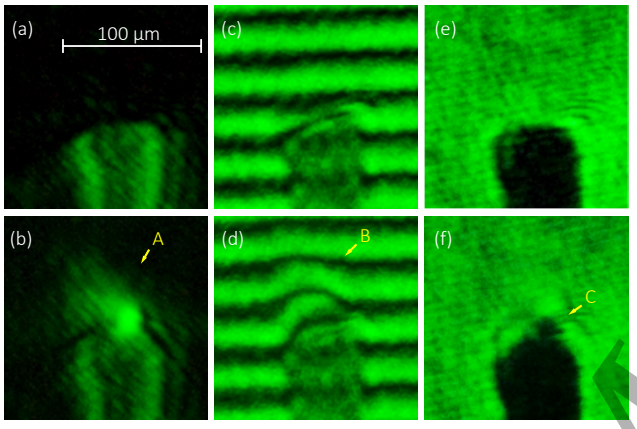

Figure 3. Shot no. 2. Schlieren-images (a,b), interferograms (c,d) and shadowgrams (e,f) obtained before discharge (a,c,e) and 1 ns (b,d,f) after breakdown; A—regions of high ($\nabla n_e \sim 10^{22}$–10^{24} cm^{-4}) electron density gradients, B—developing spark channel, C—dense ($n_e > 10^{20}$ cm^{-3}) plasma clot. Diameter of copper cathode was 50 μm.

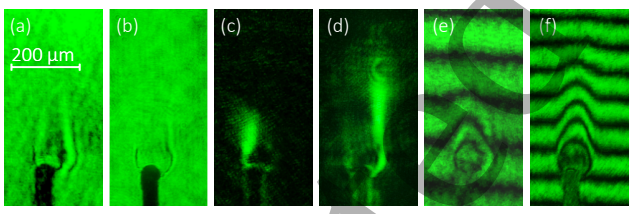

Figure 4. Shot no. 2. Shadowgrams (a,b), shlieren-images (c,d) and interferograms (e,f) of developing spark channel obtained 4 ns (a,c,e) and 5.5 ns (b,d,f) after breakdown. Images in panels (c) and (d) were obtained for different blade positions, see Fig. 1.

a plasma with an electron density of $n_e \approx 10^{19}$ cm^{-3}. During the spot formation the current is $I \sim 10$ A. Here we neglect the displacement current since it is significantly smaller than 1 A for the used geometry of the discharge gap. Remarkably, the spot size is of the same order as that of the point cathode; curvature of the latter can, in turn, result in the size limitation of the spot. Then a clot of a dense ($n_e > 10^{20}$ cm^{-3}) plasma (Fig. 3) is formed from the cathode spot with subsequent development of a highly ionized spark channel (Fig. 4) directed towards the anode. This opaque clot appears ≈ 1 ns after the breakdown and is ~ 10 μm in size. The dense plasma can be regarded as the ejection of the cathode material. Within 1–2 ns after the breakdown the near-cathode plasma, which is transparent to the probing radiation, expands in the transverse and longitudinal directions with velocities of 30 ± 5 μm/ns and 70 ± 5 μm/ns. By this time the current reaches the value of $\sim$ 100–200 A, see Fig. 5(a). It was demonstrated that the electron density is distributed non-uniformly along the spark channel (Fig. 6) and can be as high as $n_e \approx 9{\times}10^{19}$ cm^{-3}. Such extreme density is observed only within a ~ 100 μm region near the cathode and can be explained by the influence of the ionized cathode vapors as well as by strong dissociation and ionization of air molecules. Notably, Figs. 3 and 4 demonstrate only the early stage of the spark channel formation. Complete formation of the spark was traced previously in Refs. [12, 13]. In addition, the cathode-directed spark channel was not formed due to the high-quality treatment of the anode surface.

The procedure for processing the interferograms is based on solving the Helmholtz wave equation in the parabolic approximation [14]. In order to obtain the refractive index of the plasma and, thus, to reconstruct the electron density, we use the expression $n^2 = 1 - [\omega_{pe}^2/(\omega^2 + \nu_{ei}^2)](1 + i\nu_{ei}/\omega)$ [15]. Here n is the refractive index, $\omega \approx 3.5 \times 10^{15}$ s^{-1} is the frequency of the probing radiation, $\omega_{pe}^2 = 4\pi e^2 n_e/m_e$ is the plasma frequency. The frequency of ei-collisions can be taken as $\nu_{ei} = (2/3\pi)^{1/2}\omega_{pe}\Gamma_{ei}^{3/2}\Lambda_{ei}$ [15], where Λ_{ei} is the Coulomb logarithm, $\Gamma_{ei} = (Ze^2/T_e)(4\pi n_i/3)^{1/3}$ is the plasma coupling parameter, $Z = n_e/n_i$ is the average ion charge, n_i is the ion density determined by both metal and air ions. Here an important parameter for the quantitative analysis of the plasma is the electron temperature T_e. However, it is extremely difficult to obtain the information on T_e with subnanosecond temporal resolution at such a small scale by employing a direct method. Nevertheless, numerical simulations performed using the PrizmSPECT software [16] demonstrate that at $T_e \geq 3$ eV the average degree of ionization is as high as 100%. The spectral studies [17, 18] of the spark emission confirm the relevance of these numerical simulations and, hence, the average electron temperature can be taken as $T_e \approx 3$–4 eV. Given $Z \approx 1$ and the electron density up to $n_e \approx 10^{20}$ cm^{-3}, the ei-collision and plasma frequencies can be estimated as $\nu_{ei} \lesssim 10^{14}$ s^{-1} $\approx 0.2\omega_{pe}$. According to the approach developed in Refs. [19, 20, 21], the Coulomb logarithm and the plasma coupling parameter are estimated as $\Lambda_{ei} \approx 2$ and $\Gamma_{ei} \lesssim 0.35$. Consequently, both the parameter $(\nu_{ei}/\omega)^2$ and the imaginary component of

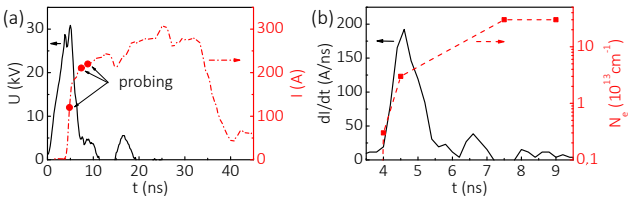

Figure 5. Discharge characteristics (a,b) in shot no. 2: U—gap voltage, I—discharge current, dI/dt—rise rate of discharge current, N_e—approximate rise curve for linear electron density; $t_{\rm br} \approx 3.5$ ns corresponds to instant of breakdown.

the refractive index are negligible and, thus, the plasma analysis is greatly simplified. Indeed, more than 90% of the probing radiation is transmitted through the spark channel.

In our work the accuracy of the electron density reconstruction is $\sim$ 10%. The sensitivity of the interferometry method is governed by the value of the minimum registered fringe shift $k_{\rm min}$. We have $k_{\rm min} = 0.1$ and the corresponding value of the minimum registered electron density is defined as $n_e^{\rm min} \approx k_{\rm min}/(A \times D \times \lambda)$. Here $A = 4.49 \times 10^{-14}$ cm is the dimensional factor, D is the channel diameter, λ is the wavelength of the probing radiation.

In spite of the fact that our findings demonstrate that the gap breakdown is associated with the appearance of the highly ionized plasma within micron-sized regions at the cathode surface, the corresponding mechanism of the plasma formation is still a subject for discussion. In this regard, let us assume that the highly ionized plasma is formed from a part of the cathode material owing to fast ($\lesssim 1$ ns) heating. In this case, the near-cathode plasma appears due to explosion of tiny (< 1 μm in size) metal spikes resulting from strong electron field emission at fields above 10^6 V/cm [22]. Indeed, numerical simulations of the electric field in the discharge gap performed using the KARAT code [23] show that at the instant of the breakdown ($U_{\rm br} \approx 20$ kV) the average electric field at the wire end is as high as $\sim 10^6$–10^7 V/cm. Moreover, the field gain at tiny spikes can be ~ 10–10^2 [4].

The advanced studies [24, 25] of a nonideal dense plasma demonstrate that during fast heating it is possible to achieve a continuous transition of a liquid metal into the state of a "supercritical fluid" avoiding the neutral vapor phase. A supercritical fluid is an intermediate state between liquid and vapor that occurs if the density, temperature and pressure are higher than the critical values $n_c \sim 10^{22}$ cm^{-3}, $T_c \sim 1$ eV, $p_c \sim 10^4$ bar. It should be noted that ions and neutral metal atoms coexist in this state. Under such conditions the conductivity of the metal $\sigma = e^2 n_e/m_e\nu$ takes the "minimum" value and the frequency of ei-collisions can be described by the Joffe-

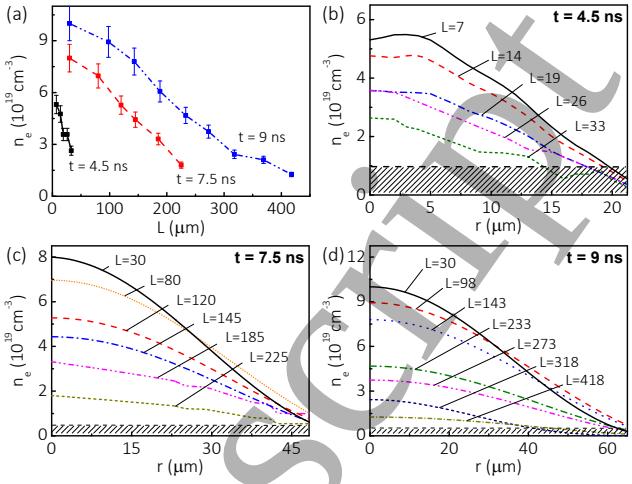

Figure 6. Distributions of electron density (n_e) along (a) and across (b,c,d) spark channel: r is transverse radius, L is distance to wire end in μm. Shaded areas correspond to electron density beyond sensitivity ($n_e^{\rm min}$) of interferometry method.

Regel formula $\nu = v_F n_c^{1/3} \sim 10^{15}$ s^{-1} [25]. Here $v_F \sim (\hbar/m_e)(3\pi^2 n_c)^{1/3} \sim 10^8$ cm/s is the electron velocity at the Fermi surface. Subsequent expansion and heating of the matter transform it to a weakly nonideal plasma with $n_e > 10^{19}$ cm^{-3}.

Thus, explosive heating of the tip of a single spike (or multiple spikes) results in the formation of the super-critical fluid with subsequent appearance of the near-cathode plasma, provided that the critical temperature is achieved. In this case, not all the spikes, but only a part of them having a certain tip curvature (r) provide for the rapid transformation of the liquid metal into the supercritical fluid. The value of r is to be consistent with the condition $r \lesssim 2\alpha/p_c \sim 1$ nm, where $\alpha \sim 10^{-3}$ N/cm is the surface tension coefficient. In this case, capillary forces compensate for the internal pressure of the liquid metal during its heating until the explosion occurs. By this time the current density attains the critical value $j = en_e c_s \sim 10^9$ A/cm^2 above which thermodynamic equilibrium between electrons and ions is broken. Here $c_s \sim (m_e/m_i)^{1/2} v_F \sim 10^5$ cm/s is the corresponding electron flow velocity. Hence, the duration of the supercritical fluid explosion is $\tau \sim n_c T_c \sigma/j^2 = 1$–$10$ ps. The explosion then expands into the remaining part of the spike. As a result, a small plasma clot composed of $\sim 10^5$ particles interacting with air molecules appears at the initial site of the spike tip with a size of $\sim 10^{-6}$ cm. This plasma expands and enhances the explosion in the region of the plasma formation and at the adjacent electron emission sites (other spikes). The explosion of several hundred spikes is sufficient to produce the plasma (Fig. 2) with the electron density of $n_e \sim 10^{19}$ cm^{-3}. Further, this plasma will expand and enhance ionization of the gas medium in the direction of the applied electric

field and, thus, promote the development of the spark channel.

The appearance of the highly ionized near-cathode plasma is essential for the initiation of the breakdown. Moreover, the dynamics of the cathode plasma governs the current capacity of the discharge gap as well as the current rise rate for ~ 1 ns after the breakdown, see Fig. 5(b). Let us justify this fact. The electron drift velocity u throughout the spark channel can be estimated as $u < v_{T_e} = (T_e/m_e)^{1/2} \sim 10^7$–$10^8$ cm/s, where v_{T_e} is the thermal velocity. The value of v_{T_e} is achieved if the electric field in the front region of the channel is as high as $E_D \approx 4\pi e^3 \Lambda_{ei} n_e/T_e \sim 10^6$ V/cm [26]. If we take the maximum possible electron drift velocity to be equal to the thermal velocity, the conduction current and its rise rate are $I \approx e v_{T_e} N_e$ and $dI/dt \approx e v_{T_e} dN_e/dt$. Here $N_e = 2\pi \int_0^{D/2} n_e(r) r dr$ is the linear electron density; D is the diameter of the spark channel. Within ~ 1 ns after the breakdown N_e reaches the value of $\sim 10^{14}$ cm^{-1} with its rise rate dN_e/dt being $\sim 10^{14}$ cm^{-1}ns^{-1}, see Fig. 5(b), and thus we obtain $I \sim 10^2$–10^3 A and $dI/dt \sim 10^2$–10^3 A/ns. Notably, if we assume T_e to be ~ 1 eV during the cathode spot formation and take the linear electron density of $N_e \sim 10^{13}$ cm^{-1} (Fig. 5), we obtain the conduction current of $I \sim 10$ A. In spite of the fact that these qualitative estimates are in agreement with the electrophysical measurements of the discharge current, we note that the current rise also depends on the ionization rate of the gas medium between the top of the spark channel and the anode. Therefore, it is important to take the high-energy electrons generated at the top of the channel (where $u \geq v_{T_e}$ holds true) into account [27]. These electrons also promote the ionization processes in the weakly ionized channel connecting the top of the spark channel and the anode [5, 28].

Thus, our findings provide a deeper insight into the initiation of a fast (~ 1 ns) air breakdown followed by the appearance of a highly ionized spark channel having the electron density of $n_e \sim 10^{19}$–10^{20} cm^{-3}. The explosive processes, namely, significant overheating of small (< 1 μm in size) metal spikes at the cathode surface, can result in fast ($\lesssim 1$ ns) formation of the plasma with an electron density $n_e \sim 10^{19}$ cm^{-3}. Our results also indicate that the highly ionized plasma generated at the cathode provides a means to manipulate the rise rate of the discharge current on a subnanosecond time scale, with the employment of additional ionization sources (e.g. laser ignition) being essential for the creation of this plasma in different regions of the cathode.

The experimental part of the study was supported by the Russian Science Foundation (grant no. 14-22-00273). The plasma analysis was partially supported by an agreement with Cornell University, Electrical and Computer Engineering, under Prime Agreement DE-NA0003764 from NNSA DOE.

References

[1] Wagenaars E 2006 *Plasma breakdown of low-pressure gas discharges* (Enschede: Eindhoven University of Technology)

[2] Walters J P 1969 *Appl. Spectrosc.* **23**(4) 317–31

[3] Bazelyan E M and Raizer Yu P 1998 *Spark Discharge* (Boca Raton, New York: CRC Press)

[4] Korolev Yu D and Mesyats G A 1998 *Physics of Pulsed Breakdown in Gases* (Ekaterinburg: Ural Division of the Russian Academy of Science)

[5] Levko D and Raja L L 2018 *Phys. Plasmas.* **25** 013509

[6] Krasik Y E, Dunaevsky A, Krokhma A, Felsteiner J, Gunin A V, Pegel I V and Korovin S D 2001 *J. Appl. Phys.* **89** 2379

[7] Juttner B 2001 *J. Phys. D* **34** R103–R123

[8] Yatom S, Vekselman V and Krasik Y E 2012 *Phys. Plasmas* **19** 123507

[9] Vasilev L 1971 *Schlieren Methods* (New York: Keter Inc.)

[10] Pikuz S A, Romanova V M, Baryshnikov N V, Hu M, Kusse B R, Sinars D B, Shelkovenko T A and Hammer D A 2001 *Rev. Sci. Instrum.* **72** 1098

[11] Volosov D S 1978 *Photographic optics* (Moscow: Iskusstvo)

[12] Parkevich E V, Tkachenko S I, Agafonov A V, Mingaleev A R, Romanova V M, Shelkovenko T A and Pikuz S A 2017 *J. Exp. Theor. Phys.* **124** 531–539

[13] Parkevich E V, Khirianova A I, Agavonov A V, Tkachenko S I, Mingaleev A R, Shelkovenko T A, Oginov A V and Pikuz S A 2018 *J. Exp. Theor. Phys.* **126** 422–429

[14] Khirianova A I, Parkevich E V and Tkachenko S I 2018 *Phys. Plasmas* **25** 073503

[15] Ginsburg V L 1970 *The Propagation of the Electromagnetic Waves in Plasma* (Pergamon: Oxford)

[16] Http://www.prism-cs.com

[17] Sukhodrev N K and Mandelstam S L 1959 *Opt. Spectrosc.* **6**

[18] Lo A, Cessou A, Lacour C, Lecordier B, Boubert P, Xu D A, Laux C O and Vervisch P 2017 *Plasma Sources Sci. Technol.* **26** 045012

[19] Bataller A, Kappus B, Camara C and Putterman S 2014 *Phys. Rev. Lett.* **113** 024301

[20] Bataller A, Plateau G, Kappus B and Putterman S 2014 *Phys. Rev. Lett.* **113** 075001

[21] Baalrud D and Daligault J 2013 *Phys. Rev. Lett.* **110** 235001

[22] Boyle W S and Haworth F E 1956 *Phys. Rev.* **101**(3) 935–938

[23] Tarakanov V P 1992 *User' s Manual for Code KARAT* (Springfield: VA: Berkley Research Associates, Inc)

[24] Clerouin J, Noiret P, Korobenko V N and Rakhel A D 2008 *Phys. Rev. B* **78** 224203

[25] Khomkin A L and Shumikhin A S 2008 *J. Exp. Theor. Phys.* **125**(6) 1189–1198

[26] Dreicer H 1959 *Phys. Rev.* **115**(2) 238–249

[27] Gurevich A V and Zybin K P 2001 *Phys.-Usp.* **44** 1119–1140

[28] Babich L P 2003 *High-Energy Phenomena in Electric Discharges in Dense Gases: Theory, Experiment and Natural Phenomena* (Arlington: Futurepast Inc.)